UCLA
COMPUTATIONAL AND APPLIED MATHEMATICS

Numerical Existence and Stability of Fluxons in a Singularly Perturbed Sine-Gordon Model of the Josephson Junction

David L. Brown
M. Gregory Forest
Brian J. Miller
N. Anders Petersson

June 1992

CAM Report 92-28

Department of Mathematics
University of California, Los Angeles
Los Angeles, CA. 90024-1555

Numerical Existence and Stability of Fluxons in a Singularly Perturbed Sine-Gordon model of the Josephson Junction

David L. Brown [1] M. Gregory Forest [2] Brian J. Miller [3]

N. Anders Petersson [4]

June 1992

[1]Computing and Communications Division and Center for Nonlinear Studies, Los Alamos National Laboratory, Los Alamos, New Mexico, USA.

[2]Computing and Communications Division, Center for Nonlinear Studies and Theoretical Division, Los Alamos National Laboratory, Los Alamos, New Mexico, USA. Permanent address: Department of Mathematics, Ohio State University, Columbus, Ohio, USA.

[3]Computing and Communications Division and Center for Nonlinear Studies, Los Alamos National Laboratory, Los Alamos, New Mexico, USA. Present address: Department of Mathematics, University of California at Los Angeles, Los Angeles, California, USA.

[4]Department of Mathematics, University of California at Los Angeles, Los Angeles, California, USA.

Abstract

In this paper, we report on some new numerical results regarding the solutions of a singularly perturbed sine-Gordon equation, modeling magnetic flux quanta (fluxons) in long Josephson tunnel junctions with non-zero surface impedance. Previous authors have conjectured that the fluxon branch of solitary wave solutions terminates at a critical value of the bias current. In the present paper, we show that the conjecture is incorrect, and that the fluxon branch of solutions may be continued. Using two different path-following bifurcation codes, we show that the critical value of the bias current corresponds not to a termination point, but to a turning point in the bifurcation diagram. Plotting a suitable norm of the solution against the bias current, we find that the solution curve turns back at the critical value and then oscillates about a limit value near the critical value while the norm of the solution increases monotonically. A careful stability analysis of these solutions shows that none of the solutions past the first turning point is stable, and that the solution acquires one additional instability per turning point. We also studied multiple fluxon solutions, i.e. solitary wave solutions which connect fixed points separated by more than 2π. The solution curves for the multiple fluxons exhibit the same qualitative behavior as those for the single fluxon case. However, the first turning point occurs at a value of the bias current which is less than the critical value. Hence, there are no solitary wave solutions when the bias current exceeds its critical value.

AMS Subject classifications: 34B15, 34C35, 34C37, 65J15, 65L07, 65L10.

Keywords: Finite difference approximation, Galilean invariance, Heteroclinic orbit, Linearized stability, Numerical continuation.

1 Introduction.

The existence of solitary wave solutions of the perturbed sine-Gordon equation,

$$\Phi_{xx} - \Phi_{tt} - \sin\Phi = \alpha\Phi_t - \beta\Phi_{xxt} - \gamma,\ \alpha > 0,\ \beta > 0,\ \gamma > 0, \tag{1}$$

is studied numerically in Forest et. al. [5]. This equation models propagation of magnetic flux quanta (fluxons) in long Josephson tunnel junctions. For the Josephson junction fluxon problem, the term in α represents shunt loss due to quasiparticle tunneling, the term in β represents dissipation due to the surface impedance of the superconducting films comprising the junction electrodes, and γ is the spatially uniform bias current normalized to the maximum zero-voltage Josephson current. Assuming a traveling wave solution of the form

$$\Phi(x,t) = \phi(x - ct) = \phi(\xi), \tag{2}$$

where c is the (unknown) propagation velocity of the fluxon, a nonlinear ODE for the fluxon shape follows, with $()'$ denoting the derivative with respect to ξ:

$$\beta c\phi'''(\xi) - (1 - c^2)\phi''(\xi) - \alpha c\phi'(\xi) + \sin\phi(\xi) - \gamma = 0. \tag{3}$$

Considering (3) in $(\phi, \phi', \phi'')^T$ phase space, the problem of computing solitary wave profiles and speeds for (1) is equivalent to finding heteroclinic orbits connecting two of the fixed points of the ODE (3). For $\gamma < 1$, (3) has two classes of fixed points:

$$\tilde{\phi}_{2j} = \arcsin(\gamma) + 2j\pi, \tag{4}$$

and

$$\tilde{\phi}_{2j+1} = \pi - \arcsin(\gamma) + 2j\pi, \tag{5}$$

where $j = 0, \pm1, \pm2, \ldots$ and $-\pi/2 \leq \arcsin(\gamma) \leq \pi/2$. For $\gamma > 1$ there are no real-valued fixed points. By linearizing (3) around a fixed point and solving the resulting ODE analytically, we get

$$\phi(\xi) = \tilde{\phi}_k + A_1 e^{\lambda_1\xi} + A_2 e^{\lambda_2\xi} + A_3 e^{\lambda_3\xi}, \tag{6}$$

where the eigenvalues are determined by the zeroes of the polynomial

$$P_\pm(\lambda) = \beta c\lambda^3 - (1 - c^2)\lambda^2 - \alpha c\lambda \pm \sqrt{1 - \gamma^2}. \tag{7}$$

The plus sign before the last term holds for the fixed points of (4) and the minus sign for those of (5). For negative c, elementary analysis shows that $P_+(\lambda)$ has one positive real zero and either two negative real zeroes or two complex conjugate zeroes with negative real part; $P_-(\lambda)$ has one negative real zero and either two positive real zeroes or two complex conjugate zeroes with positive real part. In the following, we will only consider orbits connecting the fixed points of (4).

Forest et. al. [5] computed fluxon profiles and the corresponding speeds c using a numerical shooting method. They found that for each $\gamma \leq \gamma_{crit}$ there is locally unique $\phi(\gamma)$ and $c(\gamma)$ that connects the fixed points $\tilde{\phi}_0$ and $\tilde{\phi}_2$. Numerical simulations of (1) reported by Pagano et. al. [12] showed that these single-fluxon solutions are stable. For the particular values $\alpha = 0.18$ and $\beta = 0.10$, the critical bias current is found numerically to be $\gamma_{crit} \approx 0.8877$. The authors of [5] were not able to compute trajectories connecting these fixed points for values $\gamma > \gamma_{crit}$ and the authors of [12] reported that the stable fluxon solution ceased to exist near the same

critical value of γ. For values of $\gamma > \gamma_{crit}$ the solution of (1) switches from the fluxon state to the "running mode" state. Based on their results and the consistency of these results with those reported in [12], Forest et. al. conjectured that at the value $\gamma = \gamma_{crit}$, a global bifurcation occurs, and traveling wave solutions cease to exist.

In the present paper, we report on new numerical studies that show that the conjecture in [5] is incorrect, and that the fluxon branch of solutions may be continued. Using two different path-following bifurcation codes, we show that $\gamma = \gamma_{crit}$ corresponds not to a global bifurcation point, but to a turning point in the bifurcation diagram for the problem (3). Plotting a suitable norm $\|\phi\|$ of the solution against γ, we find that the solution curve turns back at $\gamma = \gamma_{crit}$ and then oscillates about a limit value $\gamma = \gamma_{lim}$ near γ_{crit} while $\|\phi\|$ increases monotonically. An important observation is that the turning points for γ coincide with turning points for the speed c. Furthermore, c tends to the limit value $c_{lim} = -1$. A careful stability analysis of these solutions shows that none of the solutions past the first turning point is stable, and that the solution acquires one additional instability per turning point. We will also study multiple fluxon solutions of (1), i.e. solitary wave solutions which connect the fixed points $\tilde{\phi}_0$ and $\tilde{\phi}_{2j}$, $j > 1$. The solution curves for the multiple fluxons exhibit the same qualitative behavior as those for the single fluxon case. However, the first turning point occurs at a $\gamma < \gamma_{crit}$. Hence, there are no solitary wave solutions of (1) of the form (2) for $\gamma > \gamma_{crit}$.

The failure of the shooting method in [5] to find fluxon solutions past the first turning point can be traced to the extreme sensitivity of the solution to small changes in c near γ_{crit}. The failure of the dynamical simulation in [12] to find these solutions relates simply to their instability.

2 Computing the solitary wave.

The previous study of the perturbed sine-Gordon equation reported in [5] used a shooting method to compute the heteroclinic connection between the fixed points. While this method is conceptually pleasing to the dynamical systems expert, it turns out not to be the ideal way to study such problems numerically, since it is difficult to pass turning points in the solution curve such as occur in this problem. Numerical methods based on the solution of the boundary value problem (BVP) for (3) are much more robust. In this section we will discuss a new BVP method developed for this problem, and also review some of the BVP methods proposed in the literature.

Numerically, we cannot solve the problem on the infinite interval; the standard approach is to truncate the interval to, say, $a \leq \xi \leq b$, with $a < 0 < b$, and impose asymptotic boundary conditions at $\xi = a$ and $\xi = b$, cf. [10]. We seek solutions of (1) on the interval $-\infty < \xi < \infty$ that leave the fixed point $\phi = \tilde{\phi}_0$ along the one-dimensional unstable manifold and arrive at the fixed point $\phi = \tilde{\phi}_{2j}$, $j = 1, 2, 3, \ldots$, along the two-dimensional stable manifold. Number the eigenvalues such that $\Re(\lambda_1) > 0 > \Re(\lambda_2) \geq \Re(\lambda_3)$ and consider the solution of the linearized ODE (6). To get a solution that is bounded at infinity, the boundary conditions should enforce $A_1 = 0$ at $\xi = b$ and $A_2 = A_3 = 0$ at $\xi = a$. We must therefore prescribe one boundary condition at $\xi = b$ and two at $\xi = a$. Straightforward algebra yields that the requirements on A_i are satisfied if and only if the following relations are fulfilled:

$$\phi_\xi - \lambda_1(\phi - \tilde{\phi}_0) = 0, \ \xi = a, \tag{8}$$

$$\phi_{\xi\xi} - \lambda_1\phi_\xi = 0, \ \xi = a, \tag{9}$$

$$\phi_{\xi\xi} - (\lambda_2 + \lambda_3)\phi_\xi + \lambda_2\lambda_3(\phi - \tilde{\phi}_{2j}) = 0, \ \xi = b. \tag{10}$$

These relations will be used as boundary conditions for (3). We remark that from a practical

point of view, the simpler boundary conditions

$$\phi - \tilde{\phi}_0 = 0, \ \xi = a, \tag{11}$$

$$\phi_\xi = 0, \ \xi = a, \tag{12}$$

$$\phi - \tilde{\phi}_{2j} = 0, \ \xi = b. \tag{13}$$

can be used if the computational domain is sufficiently large, since the solutions decay exponentially onto the fixed point values as $|\xi| \to \infty$.

A solution of (3) at fixed c and γ is not isolated. This is due to the Galilean invariance in the ξ-direction. Let $\mathcal{L}[\phi, c, \gamma]$ be the operator described by (3). Expanding $\mathcal{L}$ around a solution $\phi^{(0)}$ yields

$$\mathcal{L}[\phi^{(0)} + \phi^{(1)}, c, \gamma] = \mathcal{L}[\phi^{(0)}, c, \gamma] + \mathcal{L}_\phi[\phi^{(0)}, c, \gamma]\phi^{(1)} + \mathcal{O}(|\phi^{(1)}|^2). \tag{14}$$

The Galilean invariance corresponds to one zero eigenvalue of $\mathcal{L}_\phi$. It is easy to see that the corresponding eigenfunction is the derivative of the present solution, i.e. $\phi^{(1)} = \phi^{(0)}_\xi$. Because of the Galilean invariance property, the solution of the problem is not completely specified by the ODE (3) and the boundary conditions (8,9,10) or (11,12,13), respectively. There are two ways to specify the solution. The first and most commonly used approach is to add one additional equation, usually called a phase constraint, to explicitly fix the phase of the solution. The second possibility, which we pursue in the present method, is to only compute the solution in the subspace which is orthogonal to the eigenfunction connected to the zero eigenvalue. Hence, we remove from the solution a one dimensional degree of freedom. By viewing the Galilean invariance in either way, it is clear that the number of free parameters is reduced from two (γ, c) to one, which we take to be γ. Thus, the velocity, c, is determined as part of the solution.

2.1 Previous methods.

The BVP-based procedures suggested by [2], [6], [9] and [11] are all based on a few simple elements. The governing solitary wave ODE is solved subject to asymptotic boundary conditions, and an additional phase constraint is imposed that fixes the location of the wave in space and also results in the unknown velocity being determined as part of the procedure. Points along the solution curve are computed using a pseudo-arclength continuation procedure. The only major difference in these methods are in the specification of the phase constraint.

In his study of solitary waves in the Fitzhugh-Nagumo equations, Miura [11] suggests a method whereby the phase is constrained by adding an additional boundary condition near the most rapidly varying part of the solitary wave profile. Since this increases the number of constraints to one more than is appropriate for a conventional BVP solver, an additional free parameter must be added. In this case it is the velocity, c. Miura implemented the method using the version of the COLSYS [1] BVP solver package available at the time. In order to arrange for an additional free parameter in that package, it was necessary to let c be a dependent variable that varied along the whole computational interval, but was constrained to be constant by adding the differential equation

$$c'(\xi) = 0. \tag{15}$$

In this approach, the solitary wave profile is the solution of the ODEs (3) and (15), subject to the boundary conditions (8,9,10) and the phase constraint

$$\phi(\frac{a+b}{2}) = \frac{\tilde{\phi}_0 + \tilde{\phi}_{2j}}{2}. \tag{16}$$

Observe that no boundary condition is necessary for c.

Kreiss [9] suggested a simplification of Miura's method in which the same phase constraint (16) is used, but the velocity c is simply allowed to be a free parameter.

The methods by Miura and Kreiss both use a point phase constraint and are therefore problem dependent, since a point on the solution profile must be chosen to be fixed. A more general approach was used by Friedman et. al. [6] and Beyn [2], who also studied the Fitzhugh-Nagumo equations. Here, the point constraint (16) is replaced by an integral constraint.

A subject which is often neglected in papers on continuation methods is how to choose a starting point. Typically, one tries to start the continuation procedure at a point where the solution can be easily computed or is known analytically. In the case of the perturbed sine-Gordon equation (3), an exact solution which connects $\tilde{\phi}_0$ and $\tilde{\phi}_2$ is given by

$$\phi(\xi) = 4 \arctan\left(e^{\xi}\right), \tag{17}$$

with $\gamma = 0$. The velocity, c, is also zero at this point, and (3) reduces to a second-order ODE. This is not an ideal starting point for the continuation procedure, because (3) is singularly perturbed for small values of c. It is our experience that this causes problems for all of the three methods discussed above.

We implemented the three methods by using AUTO [3]. When an initial guess sufficiently close to a point on the solution curve away from $\gamma = 0$ was used, all three methods functioned properly, and reproduced the results that we obtained with our method. However, without a good initial guess, AUTO diverged without being able to compute an initial point on the solution curve. Because of the singularly perturbed nature of the ODE at $\gamma = 0$, the problem specification as a first order system required by AUTO breaks down at that point, and it is necessary to start the continuation away from $\gamma = 0$. To demonstrate the sensitivity of this approach, we took $\gamma = 0.05$ together with (17) as an initial guess for the continuation. The convergence history for the first Newton iteration in Miura's method is shown in figure 1. Here, we used the simplified boundary conditions (11,12,13). Although the initial guess, labeled "iteration 0" in the figure, is very close to a solution, succeeding iterations diverge. Recall that in the pseudo-arclength continuation process, γ and c are determined as part of the computation. For each iteration, γ and c move farther away from their correct values, and although for those values, the solution curves are solutions of (3), they are not traveling wave profiles for the original problem (1). The situation becomes even worse when the asymptotic boundary conditions (8,9,10) are used (cf. fig. 2.) In this example, the initial guess

$$\phi(\xi) = \arcsin(\gamma) + 4 \arctan\left(e^{2\xi}\right). \tag{18}$$

was used. (Observe the factor 2 in the exponent, which makes the transition layer thinner than it is in the solution profile.) The Newton iterates diverge rapidly from the correct solution in this example. The asymptotic boundary conditions do not constrain the boundary values to lie near the critical points $\tilde{\phi}_0$ and $\tilde{\phi}_2$. This allows the iterates freedom to move rapidly away from the solution. This property of the asymptotic boundary conditions is discussed in more detail below.

The nonconvergence demonstrated in these tests is related to the sensitivity of the phase space topology to the value of c. For a given value of γ there is (locally) only one value of c for which a trajectory connecting the critical points exists. A small perturbation in c can cause the connection between the appropriate critical points to disappear. Neither the asymptotic

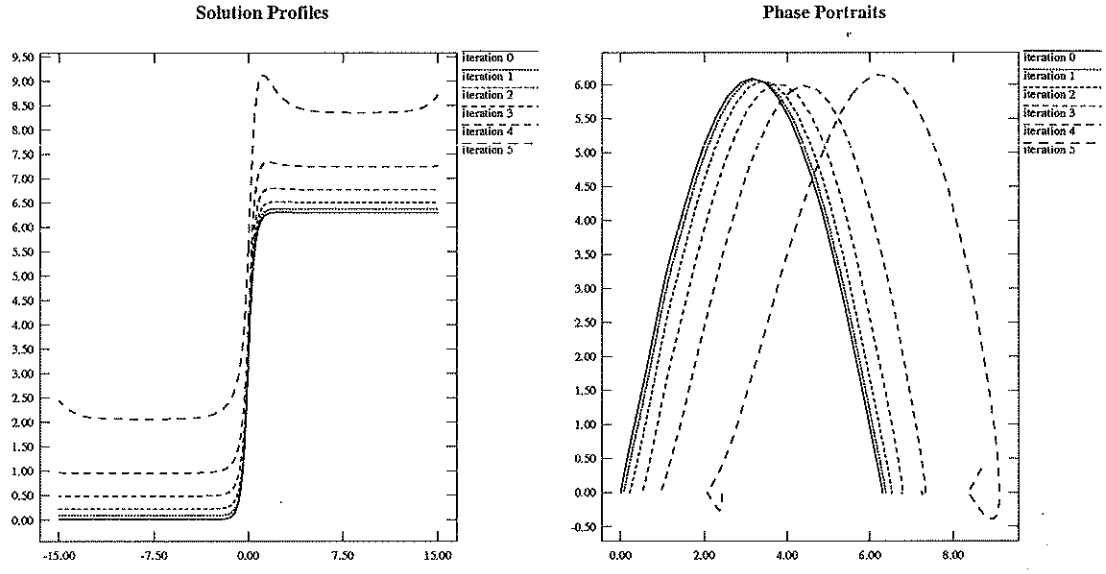

Figure 1: Iteration profiles (left) and phase portrait projected onto the (ϕ, ϕ')-plane (right) for Miura's method with an insufficiently accurate initial guess. The simplified boundary conditions (11,12,13) were used for these computations. Note that although the method computes solutions of the boundary value problem, the iterations are diverging from the desired heteroclinic orbit.

boundary conditions (8,9,10) nor the simplified boundary conditions (11,12,13) ensure that computed profiles connect points that are near the actual critical points. To do this would require six boundary conditions, and would not result in a well-posed problem. The asymptotic boundary conditions, for instance, only require that the trajectories connect a point on the linearized unstable manifold corresponding to $\tilde{\phi}_0$ (a straight line through $\tilde{\phi}_0$) with the linearized stable manifold corresponding to $\tilde{\phi}_{2j}$ (a plane containing $\tilde{\phi}_{2j}$). Thus, for given values of γ and c, it is not necessary for a trajectory connecting the critical points to exist in phase space; there is sufficient freedom in the boundary conditions for a solution to each linearized problem in the Newton iteration process to exist and be computed. It is important to realize that these solutions do not necessarily connect points in phase space near the critical points. In the example shown in figure 2, one sees in the phase portrait that although the trajectories asymptote to the appropriate linearized manifolds, they diverge from the critical points.

If in the iteration process, the iterations are not sufficiently close to the actual desired trajectories, it will often be the case that each iteration pushes the phase space topology farther and farther away from one in which a connection between the critical points exists. This is because the parameter c is computed as part of the iteration. The following analysis indicates how this can occur. Integrate the solitary wave equation (3) from $\xi = a$ to $\xi = b$. If we assume that ϕ' and ϕ'' vanish at least approximately at the endpoints of the interval, then the resulting relation may be solved for the velocity c, giving

$$c \approx \frac{1}{2\pi\alpha} \int_a^b (\sin(\phi(\xi)) - \gamma) d\xi, \tag{19}$$

for the connection between $\tilde{\phi}_0$ and $\tilde{\phi}_2$. Thus for each solution computed, the corresponding

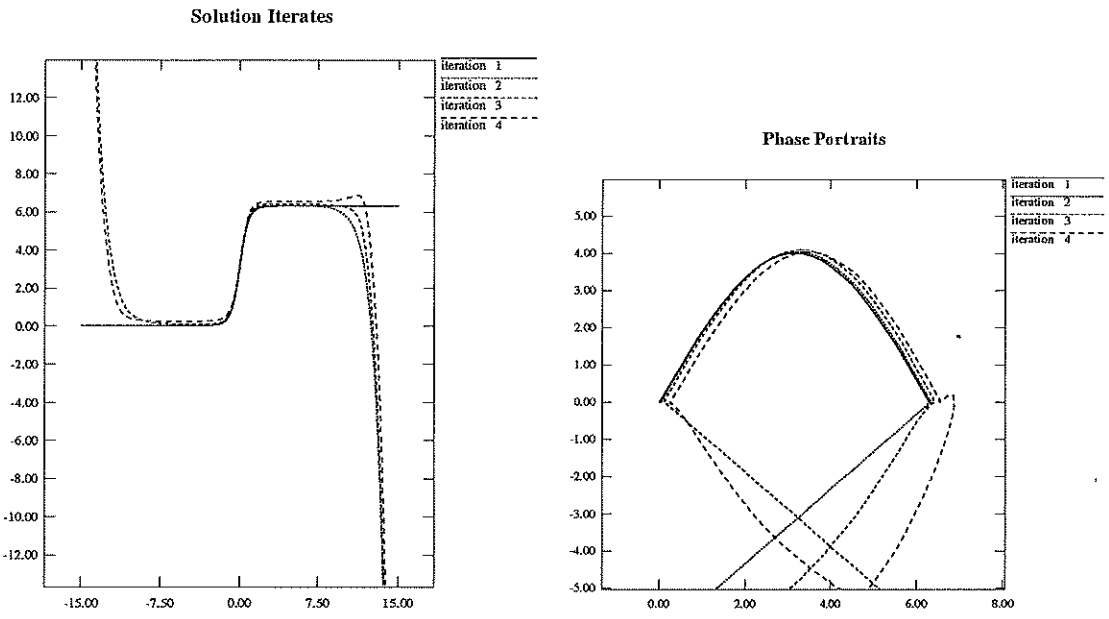

Figure 2: Iteration profiles (left) and phase portrait projected onto the (ϕ, ϕ')-plane (right) for Miura's method with an insufficiently accurate initial guess. The plots have been truncated and do not show the complete extent of the trajectories. The asymptotic boundary conditions (8,9,10) were used for these computations. The asymptotic boundary conditions only ensure that the solutions connect points on the *linearized* unstable manifold through $\phi = \tilde{\phi}_0$ with the linearized stable manifold through $\phi = \tilde{\phi}_2$. As the iterations diverge, these boundary conditions are insufficient to require that the endpoint actually be nearby the respective critical points.

velocity will depend on the area under the curve of $\sin(\phi(\xi)) - \gamma$. As soon as an iterate is computed that deviates much from the correct profile, the computed velocity can change by a large amount, thus perturbing the phase space even further, and in general convergence cannot be expected.

With these simple examples, we have demonstrated clearly the importance of a good initial guess for these solitary wave computations. We conclude this section by stating that the most reliable way to obtain a good initial guess for a solution on the solution curve is to solve the initial value problem for (1), allowing a solitary wave profile connecting the desired critical points to develop. We will discuss this approach in more detail in the section below on multiple fluxons. With this approach for obtaining the initial solution point, any of the methods that use AUTO for tracing out the solution curve will work well.

The new method we will describe below and which was used for the calculations presented in this paper, is less sensitive to the initial guess. We conjecture that its robustness is related to the way the Galilean invariance is treated.

2.2 The present method.

To find a numerical solution of (3) in $a \leq \xi \leq b$ subject to the boundary conditions (8,9,10) we approximate the ODE by a finite difference scheme. For this reason, we introduce a grid $\xi_i = a+(i-2)h$, $i = 1, \ldots, N$, where $h = (b-a)/(N-3)$; we define a grid function by $u_i = u(\xi_i)$, $i = 1, 2, \ldots, N$, and the divided difference operators by

$$D_+ u_i = \frac{u_{i+1} - u_i}{h}, \; D_- u_i = D_+ u_{i-1}, \; D_0 u_i = \frac{1}{2}(D_+ + D_-)u_i. \tag{20}$$

A second order accurate approximation of (3), i.e. $\phi(\xi_i) = u_i + \mathcal{O}(h^2)$, is given by

$$\begin{aligned} L_i =: \left(\beta c D_- D_- D_+ - (1-c^2) D_- D_0 - \alpha c D_-\right) u_i \\ + \sin\left(\frac{u_i + u_{i-1}}{2}\right) - \gamma \; = \; 0, \end{aligned} \tag{21}$$

for $i = 3, 4, \ldots, N-1$, subject to the boundary conditions

$$L_1 =: D_0 u_2 - \lambda_1 (u_2 - \tilde{\phi}_0) \; = \; 0, \tag{22}$$

$$L_2 =: D_+ D_- u_2 - \lambda_1 D_0 u_2 \; = \; 0, \tag{23}$$

$$\begin{aligned} L_N =: D_+ D_- u_{N-1} - (\lambda_2 + \lambda_3) D_0 u_{N-1} \\ + \lambda_2 \lambda_3 (u_{N-1} - \tilde{\phi}_{2j}) \; = \; 0. \end{aligned} \tag{24}$$

The discretized ODE can be viewed as a N-dimensional system of nonlinear algebraic equations. We write it in the abstract form $\boldsymbol{L}[\boldsymbol{u}, c, \gamma] = 0$ where $\boldsymbol{u} = (u_1, u_2, \ldots, u_N)^T$ and $\boldsymbol{L} = (L_1, L_2, \ldots, L_N)^T$, i.e. $\boldsymbol{L} : \mathcal{X} \times \Re \times \Re \to \mathcal{X}$ where $\mathcal{X}$ is an N-dimensional vectorspace. In the following, a triple $(\boldsymbol{u}, c, \gamma)$ that satisfies $\boldsymbol{L}[\boldsymbol{u}, c, \gamma] = 0$ will be called a solution point.

By counting the number of equations and dependent variables, it seems at first like both c and γ are free parameters. However, the Galilean invariance implies that $\boldsymbol{u}$ is only determined up to a shift. The remaining one-dimensional subspace of $\boldsymbol{u}$ must be determined by other means. In the previous methods, this is done by adding a phase constraint to fix the undetermined part of the solution. From a theoretical point of view, the phase constraint is only required to make the Jacobian of the extended system non-singular. However, it is well known that some phase constraints have better numerical properties than others [7]. To avoid the somewhat

arbitrary procedure of choosing a phase constraint, we have developed a new method which avoids adding a phase constraint. A comprehensive description of the method can be found in [13], where it was used to compute periodic water waves. To outline the method, we introduce the following notation. We define a scalar product and a norm for $x, y \in \mathcal{X}$ by $\langle x, y\rangle_h = \frac{1}{N}\sum_{i=1}^{N} x_i y_i$, $\|x\|_h = \sqrt{\langle x, x\rangle_h}$. Corresponding to the Galilean invariance, the Jacobian matrix $\partial \boldsymbol{L}/\partial \boldsymbol{u}$ will have one zero eigenvalue at every solution point. Let e_r and e_l denote the corresponding right and left eigenvectors; let them be normalized to have $\|e_r\|_h = 1$ and $\langle e_l, e_r\rangle_h = 1$. We define the projection P that maps $\mathcal{X}$ onto the eigenspace by $Pf = \langle e_l, f\rangle_h e_r$, $f \in \mathcal{X}$. The basic idea in the present method is to only solve $\boldsymbol{L} = 0$ for $(I - P)\boldsymbol{u}$, and keep $P\boldsymbol{u}$ fixed to, say, C. Obviously, the side-condition $P\boldsymbol{u} = C$ can also be viewed as a phase constraint, but this condition is derived directly from the properties of the Jacobian matrix and is therefore guaranteed to fix the phase of the solution. Furthermore, we remark that the additional cost of calculating the left and right eigenvectors is very small; they can be accurately computed with one or two iterations of the inverse power method, which is inexpensive once the Jacobian matrix has been factored.

The method can be viewed as splitting $\boldsymbol{L}$ and solving

$$(I - P)\boldsymbol{L}[\boldsymbol{u}, c, \gamma] = 0, \tag{25}$$

$$\langle e_l, \boldsymbol{L}[\boldsymbol{u}, c, \gamma]\rangle_h = 0, \tag{26}$$

for $(I - P)\boldsymbol{u}$ and c as functions of γ. The value of $P\boldsymbol{u}$ will be determined during the solution procedure. After this observation, it is clear that the number of free parameters is reduced by one, leaving one free parameter.

2.3 Continuation in γ.

To avoid complications close to turning points, we follow [8] and consider the solution $(\boldsymbol{u}, c, \gamma)$ to be a function of the pseudo-arclength s, $\boldsymbol{u} = \boldsymbol{u}(s)$, $c = c(s)$ and $\gamma = \gamma(s)$. Assume that a solution point $(\boldsymbol{u}_0, c_0, \gamma_0)$ is known, and let it have pseudo-arclength s_0. We define the pseudo-arclength relative to that point by

$$s = s_0 + \langle \dot{\boldsymbol{u}}_0, \boldsymbol{u} - \boldsymbol{u}_0\rangle_h + \dot{c}_0(c - c_0) + \dot{\gamma}_0(\gamma - \gamma_0), \tag{27}$$

where overdots denote differentiation with respect to s. The method can be outlined as follows. We seek a solution of (25–26) which has pseudo-arclength $s = s_0 + \Delta s$. First, we compute the tangent of the solution curve at the present solution point. Thereafter, we use linear extrapolation to get an initial guess for the solution at $s_0 + \Delta s$. Finally, we apply Newton's method to correct the initial guess.

The tangent $(\dot{\boldsymbol{u}}_0, \dot{c}_0, \dot{\gamma}_0)$ is the solution of

$$\begin{pmatrix} \boldsymbol{L}_{\boldsymbol{u}}[\boldsymbol{u}_0, c_0, \gamma_0] & \boldsymbol{L}_c^I[\boldsymbol{u}_0, c_0, \gamma_0] \\ \langle e_l, \boldsymbol{L}_{\boldsymbol{u}}[\boldsymbol{u}_0, c_0, \gamma_0]\rangle_h & \langle e_l, \boldsymbol{L}_c[\boldsymbol{u}_0, c_0, \gamma_0]\rangle_h \end{pmatrix} \begin{pmatrix} \dot{\boldsymbol{u}}_0 \\ \dot{c}_0 \end{pmatrix} = -\dot{\gamma}_0 \begin{pmatrix} \boldsymbol{L}_\gamma^I[\boldsymbol{u}_0, c_0, \gamma_0] \\ \langle e_l, \boldsymbol{L}_\gamma[\boldsymbol{u}_0, c_0, \gamma_0]\rangle_h \end{pmatrix}. \tag{28}$$

Here we used the notation $\boldsymbol{L}_\gamma^I[\boldsymbol{u}_0, c_0, \gamma_0] = (I - P[\boldsymbol{u}_0, c_0, \gamma_0])\boldsymbol{L}_\gamma[\boldsymbol{u}_0, c_0, \gamma_0]$. The system (28) is solved by the bordering algorithm under the side-condition $P\dot{\boldsymbol{u}}_0 = 0$ and the normalization $\|\dot{\boldsymbol{u}}_0\|_h^2 + |\dot{c}_0|^2 + |\dot{\gamma}_0|^2 = 1$.

We use the predictor $\boldsymbol{u}^0 = \boldsymbol{u}_0 + \dot{\boldsymbol{u}}_0\Delta s$, $c^0 = c_0 + \dot{c}_0\Delta s$ and $\gamma^0 = \gamma_0 + \dot{\gamma}_0\Delta s$ as initial guess for the solution at $s = s_0 + \Delta s$. The predictor is corrected by Newton's method on the augmented

system, where the improvements of the solution are found by solving

$$\begin{pmatrix} \boldsymbol{L}_{\boldsymbol{u}}[\boldsymbol{u}^k, c^k, \gamma^k] & \boldsymbol{L}_c^I[\boldsymbol{u}^k, c^k, \gamma^k] & \boldsymbol{L}_\gamma^I[\boldsymbol{u}^k, c^k, \gamma^k] \\ \langle e_l, \boldsymbol{L}_{\boldsymbol{u}}[\boldsymbol{u}^k, c^k, \gamma^k]\rangle_h & \langle e_l, \boldsymbol{L}_c[\boldsymbol{u}^k, c^k, \gamma^k]\rangle_h & \langle e_l, \boldsymbol{L}_\gamma[\boldsymbol{u}^k, c^k, \gamma^k]\rangle_h \\ N_{\boldsymbol{u}}[\boldsymbol{u}^k, c^k, \gamma^k] & N_c[\boldsymbol{u}^k, c^k, \gamma^k] & N_\gamma[\boldsymbol{u}^k, c^k, \gamma^k] \end{pmatrix} \begin{pmatrix} \Delta \boldsymbol{u}^k \\ \Delta c^k \\ \Delta \gamma^k \end{pmatrix} = - \begin{pmatrix} \boldsymbol{L}^I[\boldsymbol{u}^k, c^k, \gamma^k] \\ \langle e_l, \boldsymbol{L}[\boldsymbol{u}^k, c^k, \gamma^k]\rangle_h \\ N[\boldsymbol{u}^k, c^k, \gamma^k] \end{pmatrix}. \tag{29}$$

The arclength equation is given by

$$N[\boldsymbol{u}, c, \gamma; s] = \langle \dot{\boldsymbol{u}}_0, \boldsymbol{u} - \boldsymbol{u}_0\rangle_h + \dot{c}_0(c - c_0) + \dot{\gamma}_0(\gamma - \gamma_0) - (s - s_0). \tag{30}$$

The system (29) is solved by the bordering algorithm, under the side-condition $P[\boldsymbol{u}^k, c^k, \gamma^k]\Delta \boldsymbol{u}^k = 0$. The solution is then updated according to $\boldsymbol{u}^{k+1} = \boldsymbol{u}^k + \Delta \boldsymbol{u}^k$, $c^{k+1} = c^k + \Delta c^k$ and $\gamma^{k+1} = \gamma^k + \Delta \gamma^k$. We iterate until $\|\boldsymbol{u}^{k+1} - \boldsymbol{u}^k\|_h + |c^{k+1} - c^k| + |\gamma^{k+1} - \gamma^k| < \epsilon$. If the iteration converges, we may repeat the procedure. The number of iterations that was required to get convergence is used to determine the next step-size Δs. However, if the iteration diverges, we halve the step-size and try again.

2.4 Single fluxon.

In this section we will numerically compute the heteroclinic orbit between the fixed points $\tilde{\phi}_0$ and $\tilde{\phi}_2$. As initial guess for the continuation, we use the fluxon profile proposed by Ferrigno and Pace [4],

$$\phi(\xi) = \arcsin(\gamma) + 4\arctan\left(e^{\kappa\xi}\right), \quad \kappa = \frac{(1-\gamma^2)^{1/4}}{\sqrt{1-c^2}}. \tag{31}$$

For $\gamma = 0$ and $c = 0$, this is an exact solution of (3). As discussed in the previous section, $c \to 0$ is a singular perturbation of the ODE. We therefore need to start the continuation at non-zero c and γ. In order to estimate c for small γ, we multiply (3) by $\phi'(\xi)$ and integrate from $-\infty$ to ∞. Integration by parts and the fact that $\tilde{\phi}_{2j} - \tilde{\phi}_0 = 2j\pi$ leads to the formula

$$c = -2j\pi\gamma / \left(\alpha \int_{-\infty}^{\infty} (\phi'(\xi))^2\, d\xi + \beta \int_{-\infty}^{\infty} (\phi''(\xi))^2\, d\xi\right). \tag{32}$$

We expect the function (31) to be the leading-order approximation for small γ to the solution of (3); evaluating (32) using (31) gives the following leading order formula for c:

$$c = \frac{-3\pi\gamma}{12\kappa\alpha + 4\kappa^3\beta}. \tag{33}$$

It is desirable to measure a function ϕ which connects the fixed points $\tilde{\phi}_0$ and $\tilde{\phi}_{2j}$ in a way which is independent of the size of the computational domain. We will use the $\mathcal{L}_2$-norm of $\phi - f_j$, i.e.

$$\|\phi - f_j\|^2 = \int_{-\infty}^{\infty} (\phi(\xi) - f_j(\xi))^2\, d\xi, \tag{34}$$

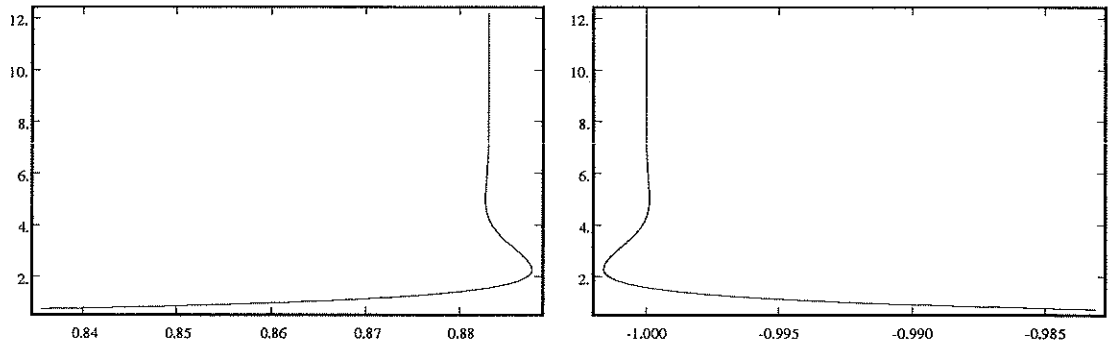

Figure 3: $\|\phi - f_1\|$ as function of γ (left) and c (right), respectively. Note that the turning points in the $\|\phi - f_1\|$-γ curve coincide within graphical accuracy to the turning points in the $\|\phi - f_1\|$-c curve.

γ	c
0.887777	-1.001666
0.882701	-0.999885
0.883051	-1.000007
0.883030	-1.000000
0.883032	-1.000000

Table 1: The first five turning points for the single fluxon.

where $f_j(\xi) = \tilde{\phi}_0 + j\pi(\tanh(\xi - \xi_0) + 1)$, with ξ_0 chosen such that $\phi(\xi_0) = \tilde{\phi}_0 + j\pi$.

We present $\|\phi - f_1\|$ versus γ and c, respectively, in figure 3. In this computation we used $\alpha = 0.18$ and $\beta = 0.10$. This choice is less restrictive than it at first might appear; a scaling law for α and β can be found in [5]. The computational domain was $-5 \leq \xi \leq 15$ and the grid had 600 grid points. No significant change in the solution was found by increasing the number of grid points further, or by making the computational domain larger.

At the first turning point, $\gamma \approx 0.887777$ and $c \approx -1.001666$. Those values coincide closely to the point past which Forest et. al. [5] were unable to find traveling wave solutions, and where Pagano et. al. [12] found that the solution of the time-dependent problem (1) switches from a traveling wave to a "running mode" state.

The solution branch has several turning points and oscillates around the limit values $\gamma_{lim} \approx 0.883032$ and $c_{lim} \approx -1.000000$, as the norm increases. The locations of the first five turning points are given in table 1. After the fifth turning point, the changes in γ and c are less than 10^{-6} along the solution curve. The solutions at the five first turning points are presented in figure 4. The part of the solution close to $\tilde{\phi}_3$ gets longer as the norm increases. Eventually, the last pass from $\tilde{\phi}_3$ to $\tilde{\phi}_2$ gets close to the end of the computational domain. Thereafter, the numerical solution has no relevance to the physical problem.

It is interesting to study the relation between γ and c close to the turning points. Refer to figure 5. Graphical accuracy suggests that $d\gamma/dc$ does not exist at the turning point, which only

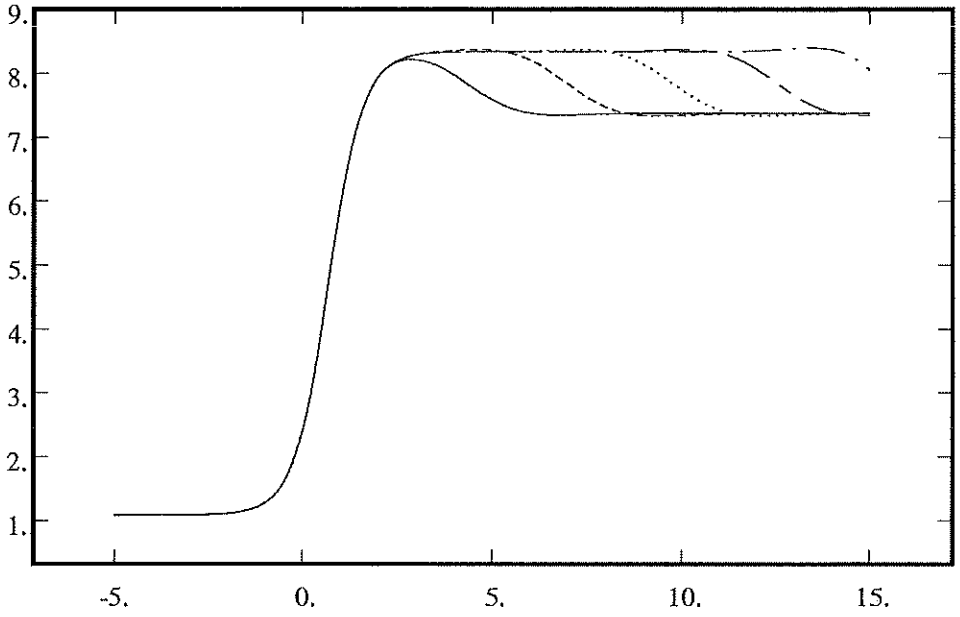

Figure 4: ϕ as function of ξ at the five first turning points for the single fluxon. The solid line corresponds to the first turning point.

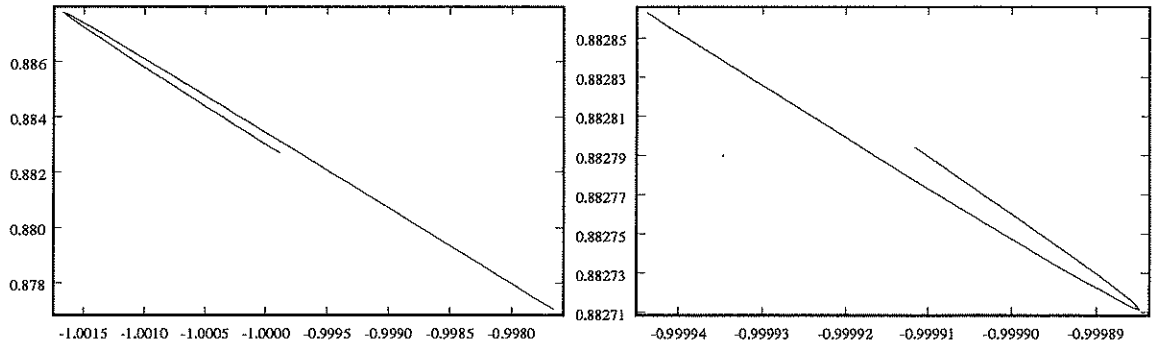

Figure 5: The relation between γ (vertical axis) and c (horizontal axis) close to the first (left) and the second (right) turning point for the single fluxon.

can happen if the turning points in c and γ coincide. To pursue this question further, we take $j = 1$ and differentiate (32) with respect to arclength, i.e.

$$\frac{dc}{ds} = -2\pi \left(\frac{1}{\|\phi\|_H^2} \frac{d\gamma}{ds} - \frac{\gamma}{\|\phi\|_H^4} \frac{d\|\phi\|_H^2}{ds} \right), \quad \|\phi\|_H^2 = \alpha(\phi', \phi') + \beta(\phi'', \phi''), \tag{35}$$

where we define the inner product for functions f and g in $\mathcal{L}_2$ by $(f, g) = \int_{-\infty}^{\infty} \bar{f} g \, d\xi$. We want to show that a turning point in γ implies a turning point in c, i.e. that $\dot{c} = 0$ if $\dot{\gamma} = 0$. Obviously, this can only happen if also $d\|\phi\|_H^2/ds = 0$ at the turning point. Differentiating $\|\phi\|_H^2$ with respect to s and integrating by parts yields,

$$\frac{d\|\phi\|_H^2}{ds} = 2 \left(\frac{d\phi}{ds}, \beta\phi^{(IV)} - \alpha\phi'' \right). \tag{36}$$

By differentiating (3) with respect to ξ and substituting $\beta\phi^{(IV)} - \alpha\phi''$, we find

$$\frac{d\|\phi\|_H^2}{ds} = \frac{2}{c} \left(\frac{d\phi}{ds}, (1 - c^2)\phi''' - \phi' \cos\phi \right). \tag{37}$$

At the turning point, $\mathcal{L}_\phi$ has two zero eigenvalues, which means that there is a nontrivial solution $\psi \neq \phi'$ of

$$\beta c\psi''' - (1 - c^2)\psi'' - \alpha c\psi' + \psi \cos\phi = 0. \tag{38}$$

In addition, it is easy to see that $\psi = d\phi/ds$ at the turning point. By (38), $\psi \cos\phi = -\beta c\psi''' + (1 - c^2)\psi'' + \alpha c\psi'$. Substituting this into (37) and integrating by parts yields

$$\frac{d\|\phi\|_H^2}{ds} = 2(\phi', \beta\psi''' - \alpha\psi') = 2(\psi, \alpha\phi'' - \beta\phi^{(IV)}). \tag{39}$$

Adding (36) and (39) gives $d\|\phi\|_H^2/ds = 0$, which proves the assertion.

2.5 Multiple fluxons.

It is possible to construct a heteroclinic orbit between $\tilde{\phi}_0$ and $\tilde{\phi}_{2j}$ for $j > 1$ by using widely separated single fluxons. For instance, a connection between $\tilde{\phi}_0$ and $\tilde{\phi}_4$ is given by

$$\phi(\xi) = \lim_{\xi_0 \to \infty} \begin{cases} \psi(\xi + \xi_0), & \xi \leq 0 \\ \tilde{\phi}_2 + \psi(\xi - \xi_0), & \xi > 0 \end{cases}, \tag{40}$$

where $\psi(\xi)$ is a single fluxon with $\psi(0) = \tilde{\phi}_0 + \pi$. In this section, we will compute another family of solitary waves that connect $\tilde{\phi}_0$ and $\tilde{\phi}_{2j}$ for $j > 1$.

In contrast to the single fluxon case, initial data for the continuation is not available in the form of analytical expressions. Instead, we will integrate the solution of (1) in time at a fixed value of γ until a solitary wave has formed, and start the continuation from that profile.

It is possible to rewrite (1) as a first order system of standard type by introducing new dependent variables u and v by $\Phi_t = (v - u)/\beta$ and $\Phi = u$. This gives

$$\begin{pmatrix} u \\ v \end{pmatrix}_t = \begin{pmatrix} 0 & 0 \\ 0 & \beta \end{pmatrix} \begin{pmatrix} u \\ v \end{pmatrix}_{xx} + \begin{pmatrix} -1/\beta & 1/\beta \\ \alpha - 1/\beta & -\alpha + 1/\beta \end{pmatrix} \begin{pmatrix} u \\ v \end{pmatrix} + \beta \begin{pmatrix} 0 \\ \gamma - \sin u \end{pmatrix}, \tag{41}$$

γ_2	c_2	γ_3	c_3
0.871963	-1.001754	0.871099	-1.001476
0.866099	-0.999872	0.866173	-0.999896
0.866524	-1.000008	0.866520	-1.000007
0.866498	-0.999999	0.866499	-1.000000
0.866500	-1.000000	0.866450	-1.000000

Table 2: The first five turning points for the cases $j = 2$ and $j = 3$. Note that the first turning point for the single fluxon case occurs at a larger value of γ than it does here.

which is a well-posed mixed hyperbolic-parabolic system. To avoid interactions between the solitary wave and any boundaries, we approximate the infinite domain by a periodic domain with large period. Let the infinite domain be truncated to $a \leq x \leq b$, $a < 0 < b$. At the boundaries, we impose $\Phi(b,t) = \Phi(a,t) + 2j\pi$ and $\Phi_t(b,t) = \Phi_t(a,t)$, which expressed in u and v corresponds to

$$u(b,t) = u(a,t) + 2j\pi, \tag{42}$$
$$u_x(b,t) = u_x(a,t), \tag{43}$$
$$v(b,t) = v(a,t) + 2j\pi, \tag{44}$$
$$v_x(b,t) = v_x(a,t). \tag{45}$$

This system is discretized in space with second order accurate centered finite differences, and the resulting system of ODEs is integrated in time using a four stage, fourth order, Runge-Kutta scheme. As initial value, we use the single kink from $\tilde{\phi}_0$ to $\tilde{\phi}_{2j}$ given by

$$u(x,0) = \tilde{\phi}_0 + 4j \arctan(e^x), \tag{46}$$
$$v(x,0) = \tilde{\phi}_0 + 4j \arctan(e^x). \tag{47}$$

The profile of the solution will be translated in space as time evolves. Because of the jump by $2j\pi$ in the boundary conditions, u and v will increase by $2j\pi$ every time the wave travels across the boundary. The profile from the time-dependent calculation, $u(x,T)$, must therefore be corrected before it becomes useful as initial guess for the continuation. We do this by shifting the profile in x to move the kink close to $x = 0$ and adding a constant such that $u(a,T) = \tilde{\phi}_0$. We then start the continuation at $\phi^0(\xi) = u(\xi,T)$. The corresponding value of c is calculated by using (32).

As in the single fluxon case, we used $\alpha = 0.18$ and $\beta = 0.10$ in the numerical calculations. To get a starting point for the continuation, we took $\gamma = 0.75$ and integrated (41) up to time $t = 30$. The computational domain was between $a = -5.0$ and b=20.0 and the grid had 750 grid points, which corresponds to the same grid size as in the single fluxon case.

Qualitatively, the curves $\|\phi - f_j\|$ versus γ and c, for $j = 2$ and $j = 3$, closely resemble those for $j = 1$. The locations of the first five turning points are given in table 2, where γ_j and c_j correspond to the orbit between $\tilde{\phi}_0$ and $\tilde{\phi}_{2j}$. We emphasize one important physical consequence of table 1 and 2. The value of γ at the first turning point for the multiple fluxon is smaller than it is at the first turning point for the single fluxon, where $\gamma = \gamma_{crit}$. Hence, multiple fluxons

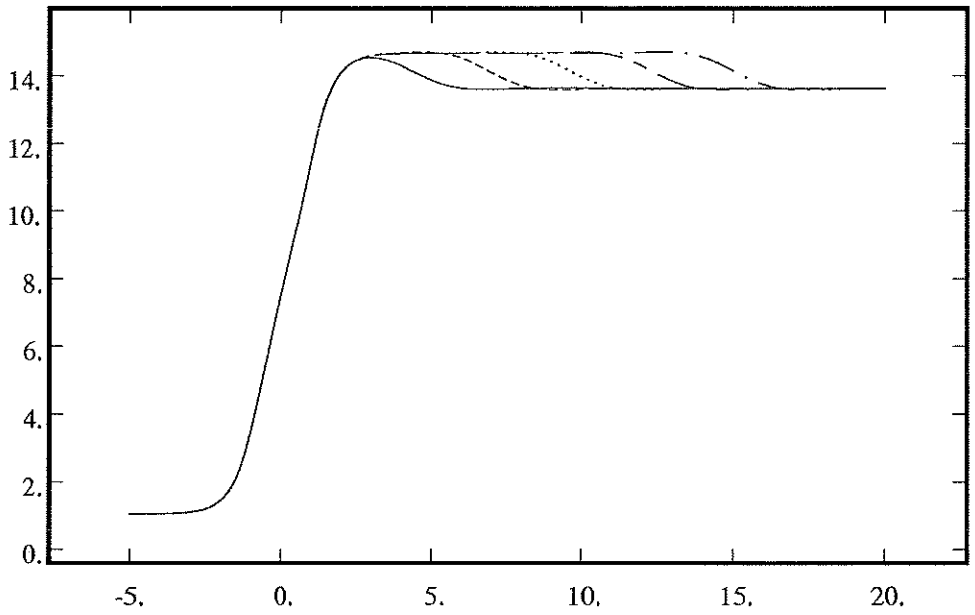

Figure 6: The case $j = 2$. ϕ as function of ξ at the five first turning points. The solid line corresponds to the first turning point.

do not exists for $\gamma > \gamma_{crit}$ so there are no solitary wave solutions in that regime. This fact is consistent with the dynamical studies in [12], where the solution was observed to switch to a "running mode" state for $\gamma > \gamma_{crit}$.

The solutions at the five first turning points for $j = 2$ are presented in figure 6 and for $j = 3$ in figure 7.

3 Stability.

Pagano et. al. [12] found that the time-dependent solution of (1) switches from a solitary wave to a "running mode" state when γ exceeds a critical value close to where we found the first turning point. This observation suggests that the solitary wave solutions are unstable past the first turning point. In this section, we will investigate the stability of the solitary wave by computing the spectrum of the linearized operator.

It is convenient to consider the time dependent problem (1) written as a hyperbolic-parabolic system (41). In a reference frame where the solitary wave is steady, it becomes

$$\begin{pmatrix} u \\ v \end{pmatrix}_\tau = \begin{pmatrix} c\partial/\partial\xi - 1/\beta & 1/\beta \\ \alpha - 1/\beta & \beta\partial^2/\partial\xi^2 + c\partial/\partial\xi - \alpha + 1/\beta \end{pmatrix} \begin{pmatrix} u \\ v \end{pmatrix} + \beta \begin{pmatrix} 0 \\ \gamma - \sin u \end{pmatrix}, \quad (48)$$

where $\xi = x - ct$ and $\tau = t$. Let the solitary wave solution of (3) be $\phi_0(\xi)$. This solution is equivalent to a steady solution of (48) with $u_0 = \phi_0$ and $v_0 = \phi_0 - \beta c\partial\phi_0/\partial\xi$. We linearize (48) by inserting the ansatz $u(\xi,\tau) = u_0(\xi) + u_1(\xi,\tau)$, $v(\xi,\tau) = v_0(\xi) + v_1(\xi,\tau)$ and neglecting terms quadratic in u_1 and v_1. The eigenvalue problem is found by assuming $u_1(\xi,\tau) = u_2(\xi)\exp(\lambda\tau)$ and $v_1(\xi,\tau) = v_2(\xi)\exp(\lambda\tau)$. We arrive at

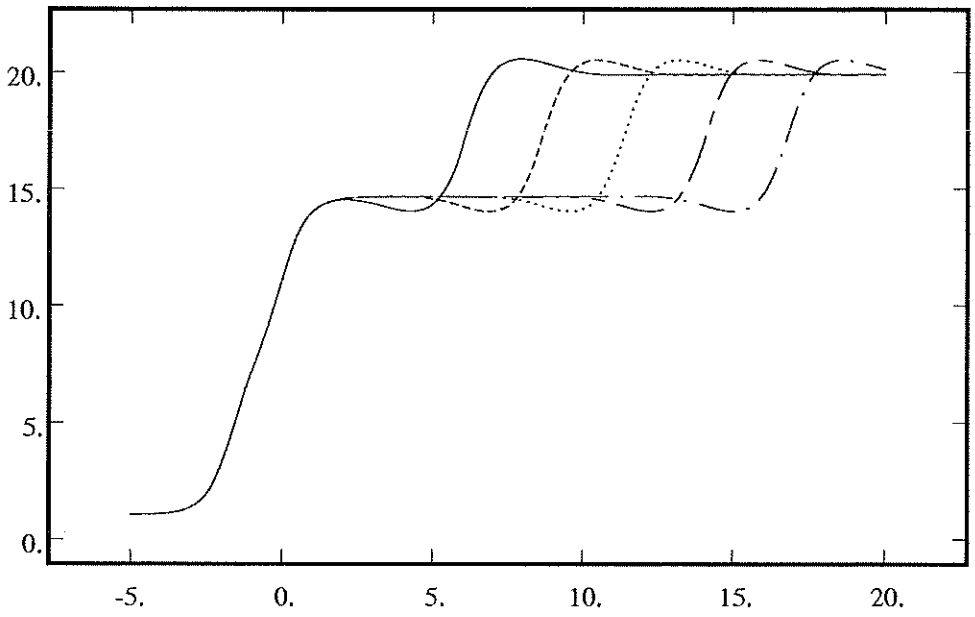

Figure 7: The case $j = 3$. ϕ as function of ξ at the five first turning points. The solid line corresponds to the first turning point.

$$\lambda \begin{pmatrix} u_2 \\ v_2 \end{pmatrix} = \begin{pmatrix} c\partial/\partial\xi - 1/\beta & 1/\beta \\ \alpha - 1/\beta - \beta\cos u_0 & \beta\partial^2/\partial\xi^2 + c\partial/\partial\xi - \alpha + 1/\beta \end{pmatrix} \begin{pmatrix} u_2 \\ v_2 \end{pmatrix}. \tag{49}$$

We will refer to (49) as the continuous variable coefficient eigenvalue problem.

A solution of (48) is said to be *linearly stable* if all eigenvalues λ of the problem (49) have non-positive real part. The eigenvalues and the eigenfunctions are continuous functions of the arclength along the solution curve. If a solution is linearly stable at one solution point, it can only lose stability if one or more eigenvalues crosses the imaginary axis $\Re(\lambda) = 0$. The loss of stability in the present problem is apparently associated with the first turning point of the solution curve for the traveling wave problem. We will therefore study the stability of the solutions close to that point. We will also study the stability of solutions between succeeding turning points. Our conclusions from numerical and analytical studies of the eigenvalue problem can be summarized as follows: For single fluxon solutions before the first turning point, all eigenvalues of (49) have non-positive real part. Thus, those solutions are linearly stable. Loss of stability occurs at the first turning point when one eigenvalue crosses the imaginary axis. At each succeeding turning point, an additional eigenvalue crosses the imaginary axis; thus, stability is never regained beyond the first turning point. The behavior of multiple fluxon solutions is similar: linear stability is lost at the first turning point, and each succeeding turning point corresponds to another eigenvalue crossing the imaginary axis. An important point to note is that the first turning point for each of the multiple fluxon solutions occurs at a γ which is always less than the critical value of γ for the single fluxon solution. Thus, there are apparently no linearly stable solutions of (48) for values of γ greater than the value at the first turning point of the single fluxon solution curve.

We demonstrate these summarized results by a careful analysis on both the discrete and the continuous eigenvalue problems related to the continuous variable coefficient eigenvalue problem

(49). The spectrum of a continuous operator is well-approximated by the corresponding discrete operator only for those eigenfunctions that can be well-represented on the computational mesh used for the discretization. Typically, these eigenfunctions correspond to eigenvalues with small absolute value. It is necessary to use analytical arguments to describe the other parts of the spectrum. In the following, we show that the spectrum of some related constant coefficient operators which can be determined exactly are in a certain limit identical to parts of the spectrum for the variable coefficient problem. The rest of the spectrum appears to consist of eigenvalues corresponding to localized eigenfunctions that occur only in the variable coefficient problem; these are also the eigenvalues critical to determining linearized stability. These localized eigenfunctions are well-represented on a finite-difference mesh, and thus can be determined numerically along with the corresponding eigenvalues.

To study the stability numerically, we truncate the infinite domain to a finite domain $a \le \xi \le b$, $a < 0 < b$, and assume the perturbation (u_2, v_2) to be periodic in ξ, i.e. $u_2(\xi) = u_2(\xi + b - a)$ and $v_2(\xi) = v_2(\xi + b - a)$. We discretize (49) on a grid $\xi_j = a + jh$, $h = (b-a)/N$, where a gridfunction is defined by $(u_2(\xi_j), v_2(\xi_j)) = (u_{2,j}, v_{2,j})$. The derivatives in (49) are approximated by the previously introduced divided difference operators. This procedure results in the matrix eigenvalue problem,

$$\kappa \begin{pmatrix} u_{2,j} \\ v_{2,j} \end{pmatrix} = \begin{pmatrix} cD_0 - 1/\beta & 1/\beta \\ \alpha - 1/\beta - \beta \sin u_{0,i} & \beta D_+ D_- + cD_0 - \alpha + 1/\beta \end{pmatrix} \begin{pmatrix} u_{2,j} \\ v_{2,j} \end{pmatrix}, \tag{50}$$

for $j = 1, 2, \ldots, N$, with the boundary conditions $(u_{2,0}, v_{2,0}) = (u_{2,N}, v_{2,N})$ and $(u_{2,N+1}, v_{2,N+1}) = (u_{2,1}, v_{2,1})$. Henceforth, (50) will be called the discrete variable coefficient eigenvalue problem.

To better understand the behavior of the spectrum, and to check the numerical calculation, it is helpful to replace the variable coefficient $\sin u_0(\xi)$ by its value at the fixed points, $\sin \tilde{\phi}_0 = \sin \tilde{\phi}_{2j}$, $j \ge 1$. Since the coefficients in the problem are constant, it is possible to solve the eigenvalue problems (49) and (50) analytically. Those problems will be denoted the continuous and the discrete constant coefficient eigenvalue problems, respectively. In both cases, the eigenfunctions are given by $\exp(i\omega_k(x-a))$, $\omega_k = 2\pi k/(b-a)$, $k = 0, \pm 1, \pm 2, \ldots$. The eigenvalues of the continuous constant coefficient problem are given by

$$\tilde{\lambda}_k = -\frac{\alpha + \beta\omega_k^2}{2} + i\omega_k c \pm \sqrt{\left(\frac{\alpha + \beta\omega_k^2}{2}\right)^2 - \omega_k^2 - \cos\tilde{\phi}_0}. \tag{51}$$

The eigenvalues of the discrete constant coefficient problem are given by

$$\tilde{\kappa}_k = -\frac{\alpha + \beta\sigma_k^2}{2} + i\rho_k c \pm \sqrt{\left(\frac{\alpha + \beta\sigma_k^2}{2}\right)^2 - \sigma_k^2 - \cos\tilde{\phi}_0}, \tag{52}$$

where $\sigma_k = 2\sin(\omega_k h/2)/h$ and $\rho_k = \sin(\omega_k h)/h$. In the discrete case, the number of eigenfunctions which are unique on the grid is equal to the number of grid points, N. For even N, we will use $-N/2 + 1 \le k \le N/2$.

The spectra for the continuous variable and constant coefficient problems are closely related. This will be demonstrated in the case when the variable coefficient only varies in the interval $a_1 < x < b_1$, i.e. $\cos u_0(x) - \cos\tilde{\phi}_0 = 0$ in $a \le x < a_1$, $b_1 < x \le b$, where a_1 and b_1 are independent of a and b. However, the result can be generalized to the case where the variable coefficient decays exponentially outside $a_1 \le x \le b_1$. We will show that for each eigenvalue $\tilde{\lambda}$ of the constant coefficient problem, there is an eigenvalue λ of the variable coefficient problem with

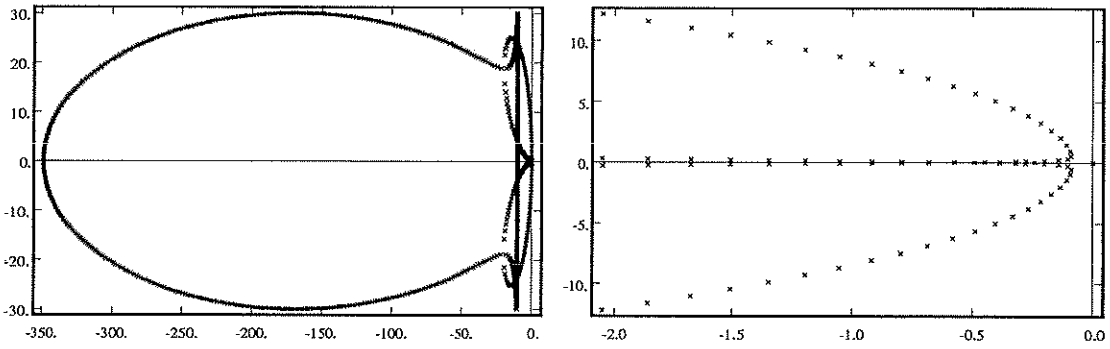

Figure 8: The spectrum of the discrete variable coefficient problem (50) close to the first turning point of the single fluxon. The real part of the eigenvalue corresponds to the horizontal axis; the imaginary part corresponds to the vertical axis. To the left we show all eigenvalues, and to the right we present an enlargement close to the origin.

$|\lambda - \tilde{\lambda}| = \mathcal{O}(\epsilon)$, $\epsilon = (b_1 - a_1)/(b - a)$. Hence, it is possible to make $|\lambda - \tilde{\lambda}|$ as small as we please by increasing the period, $b - a$. Let $A\bar{u} = \lambda\bar{u}$, $\bar{u} = (u, v)^T$, denote the variable coefficient eigenvalue problem (49), and $A_0\bar{u}_0 = \tilde{\lambda}\bar{u}_0$ denote the corresponding constant coefficient eigenvalue problem. We assume an asymptotic expansion of the form

$$\begin{aligned} \lambda &= \tilde{\lambda} + \epsilon\lambda', \\ \bar{u} &= \bar{u}_0 + \epsilon\bar{u}'. \end{aligned} \tag{53}$$

The eigenvalue is determined by the Rayleigh quotient $\lambda = (\bar{u}, A\bar{u})_2/(\bar{u}, \bar{u})_2$, where the scalar product for functions $\bar{w}_j = (u_j, v_j)^T$ in $\mathcal{L}_2$ is defined by $(\bar{w}_1, \bar{w}_2)_2 = (u_1, u_2) + (v_1, v_2)$. By inserting the asymptotic expansion (53) in the Rayleigh quotient, we get

$$\lambda' = \frac{(\bar{u}', A_0\bar{u}_0)_2}{(\bar{u}_0, \bar{u}_0)_2} + \frac{(\bar{u}_0, A_1\bar{u}_0)_2}{\epsilon(\bar{u}_0, \bar{u}_0)_2} + \frac{(\bar{u}', A_1\bar{u}_0)_2}{(\bar{u}_0, \bar{u}_0)_2} + \frac{(\bar{u}_0, A_0\bar{u}')_2}{(\bar{u}_0, \bar{u}_0)_2} - 2\tilde{\lambda}\frac{(\bar{u}_0, \bar{u}')_2}{(\bar{u}_0, \bar{u}_0)_2} + \mathcal{O}(\epsilon), \tag{54}$$

where $A_1 = A - A_0$. We complete the proof by using $|\cos u_0(x) - \cos\tilde{\phi}_0| \leq 2$, $a_1 \leq x \leq b_1$, and $\bar{u}_0 \sim \exp(i\omega x)$ to show $|(\bar{u}_0, A_1\bar{u}_0)_2| \leq \beta\epsilon(\bar{u}_0, \bar{u}_0)_2$. Hence, $\lambda' \leq C$, where C is independent of ϵ.

In the constant coefficient problem, the distance between consecutive eigenvalues, $|\tilde{\lambda}_{k+1} - \tilde{\lambda}_k|$, decreases when the period, $b - a$, increases. In the limit when the period tends to infinity, those eigenvalues form a continuous spectrum. In the same limit, $|\lambda - \tilde{\lambda}|$ tends to zero. Thus, the continuous spectra are identical for the constant and variable coefficient problems. However, there might be additional eigenvalues in the variable coefficient problem that are not present in the constant coefficient problem; these eigenvalues must be computed numerically.

Similar to the previous computations, we used $\alpha = 0.18$, $\beta = 0.10$. The spectrum of the discrete variable coefficient problem (50) was numerically computed with the routine RG in the SLATEC library. That spectrum, at the first turning point for the single fluxon, is given in figure 8. At that point, $\gamma \approx 0.887777$ and $c \approx -1.001666$. The computational domain was between $a = -5.0$ and $b = 15.0$; the grid had 600 grid points. We would like to know how close the eigenvalues of the discrete variable coefficient problem are to the corresponding continuous problem. From the previous analysis, we know that the spectrum of the continuous variable coefficient problem is similar to that of the corresponding constant coefficient problem. We will

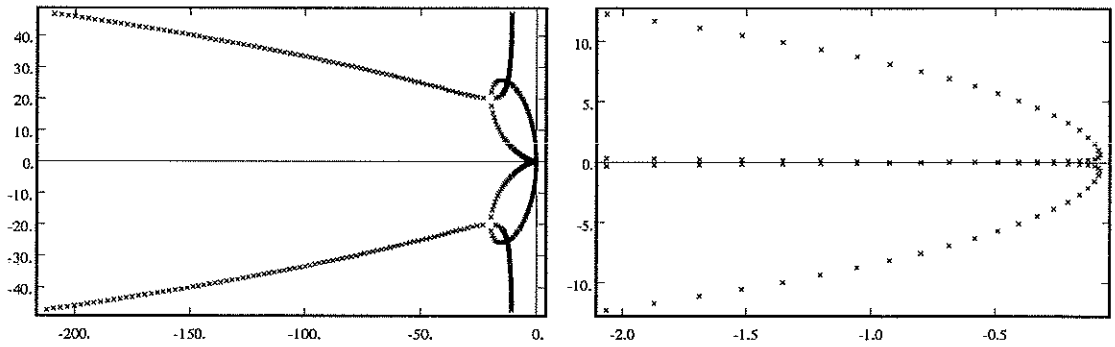

Figure 9: The spectrum of the continuous constant coefficient problem (51) at the first turning point. In this calculation, $a = -5.0$ and $b = 15.0$. To the left we show the eigenvalues corresponding to $-150 \leq k \leq 150$, and to the right we present an enlargement close to the origin.

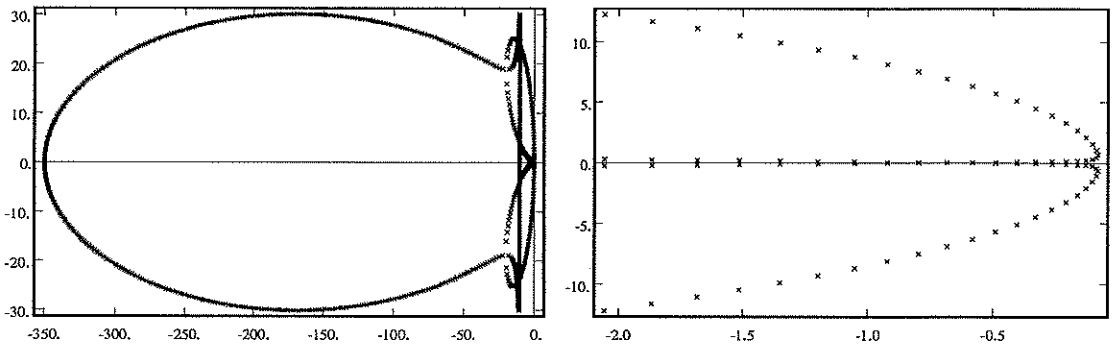

Figure 10: The spectrum of the discrete constant coefficient problem (52) at the first turning point. In this calculation, $N = 600$, $a = -5.0$ and $b = 15.0$. To the left we show all eigenvalues, and to the right we present an enlargement close to the origin.

therefore get a good understanding of the differences between the eigenvalues of the continuous and discrete variable coefficient problems by studying the corresponding constant coefficient problems. We present the spectrum of the continuous constant coefficient problem (51) at the first turning point in figure 9. The spectrum of the discrete constant coefficient problem (52) for the same case is depicted in figure 10. Many features of the spectrum of the continuous constant coefficient problem are captured by the spectrum of the discrete constant coefficient problem. However, the discrepancies grow when the magnitudes of the real or imaginary parts increase. There is also a line of eigenvalues with real part ≈ -10 in the spectrum of the discrete problem which does not exist in the continuous case. Those parts of the spectrum have large values of ω_k, and correspond to spurious numerical eigenfunctions that are highly oscillatory on the grid.

The spectrum of the discrete constant coefficient problem is very similar to that of the discrete variable coefficient problem. The only significant differences are close to the origin, where the variable coefficient problem has a number of eigenvalues which are absent in the constant coefficient spectrum. For instance, there are two eigenvalues $\kappa = 0$. One of them corresponds

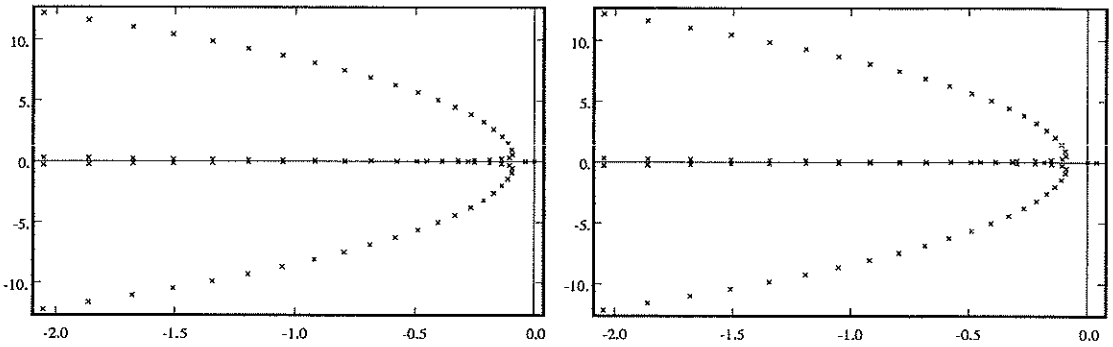

Figure 11: The eigenvalues of smallest magnitude of (50) just before the first turning point (left) and just after it (right). In this calculation, $N = 600$, $a = -5.0$ and $b = 15.0$. Note that one eigenvalue passes the imaginary axis.

to the Galilean invariance, and the other corresponds to the turning point itself. We conjecture that the spectrum for the continuous variable coefficient problem can be well approximated by the continuous constant coefficient problem for large $|\lambda|$ and by the discrete variable coefficient problem for small $|\lambda|$.

We now study the spectrum corresponding to the single fluxon at different locations along the solution curve. Recall that if a solution is linearly stable at one solution point, it can only loose stability if one or more eigenvalues passes the imaginary axis $\Re(\kappa) = 0$. In figure 11, we present the spectra connected to one solution point just before the first turning point and one just after it. One eigenvalue gets a positive real part after the turning point, which means that the solitary wave acquires a one-dimensional instability. The eigenvector connected to that eigenvalue is depicted in figure 12. The spectrum close to the second turning point is shown in figure 13. Here, the real part of one more eigenvalue becomes positive. This pattern repeats at the subsequent turning points, so that the solution never regains linear stability. Instead, the unstable manifold grows by one dimension past each turning point along the solution curve. The eigenvalues of the multiple fluxons behave in the same way. We conclude that the solitary wave solutions are linearly unstable past the first turning point. This explains why these solutions were not observed in the dynamical studies [12].

4 Acknowledgments.

The authors are grateful to Heinz-Otto Kreiss and Jens Lorenz for interesting and helpful discussions. Some of the calculations discussed in this paper were done with AUTO, which was provided to us by Eusebius Doedel, to whom we also express our thanks for his help in adapting the code to our purposes. This work was partially supported by the U.S. Department of Energy through Los Alamos National Laboratory under contract W-7405-ENG-36.

NAP also acknowledges the support from ONR grants N-00014-90-J-1695 and N-00014-90-J-1382.

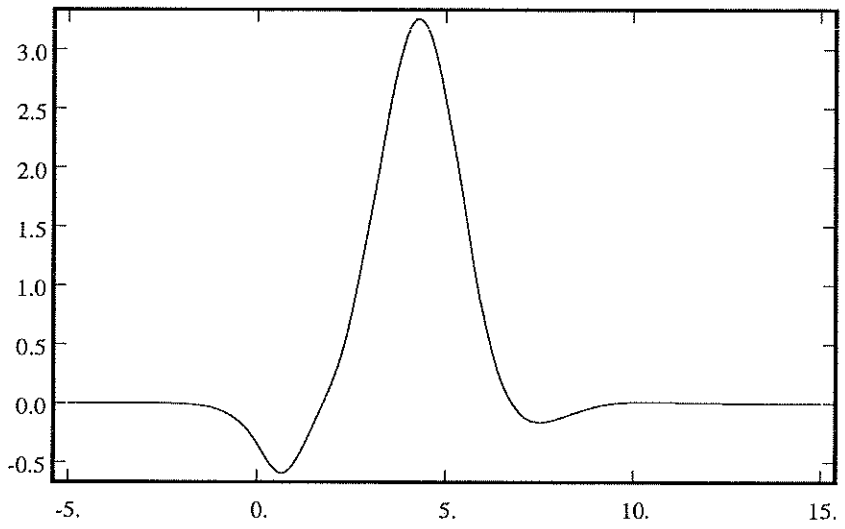

Figure 12: The u-component of the eigenvector of (50) corresponding to the eigenvalue which real part changes sign at the first turning point. Here, $N = 600$, $a = -5.0$, $b = 15.0$, $\gamma \approx 0.887777$ and $c \approx -1.001666$.

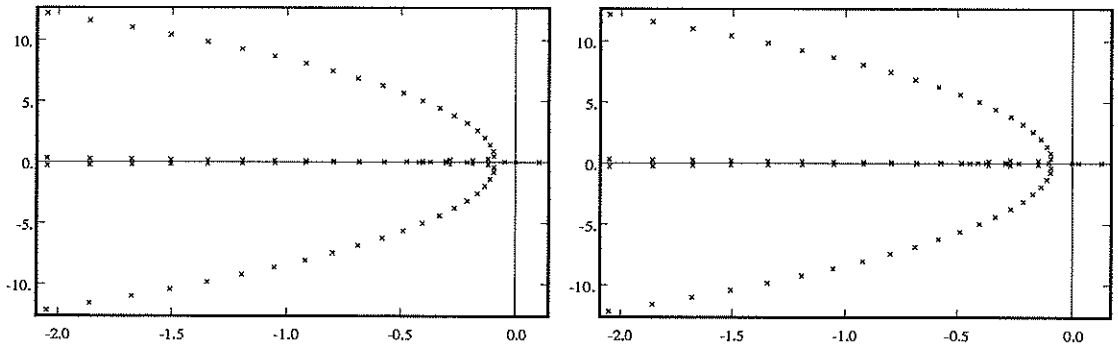

Figure 13: The eigenvalues of smallest magnitude of (50) just before the second turning point (left) and just after it (right). In this calculation, $N = 600$, $a = -5.0$ and $b = 15.0$. Note that two eigenvalues have positive real part after the turning point.

References

[1] U. Ascher, J. Christiansen, and R.D. Russell, Collocation software for boundary value ODEs, *ACM Trans. Math. Software*, **7**, (1981), pp. 209-222.

[2] W.-J. Beyn, The numerical computation of connecting orbits in dynamical systems, *IMA J. Numer. Anal.*, **9**, (1990), pp. 379-405.

[3] E.J. Doedel and J.P. Kernévez, AUTO: software for continuation and bifurcation problems in ordinary differential equations, (Applied Mathematics Report, California Institute of Technology, Los Angeles, CA, 1986).

[4] A. Ferrigno and S. Pace, *Phys. Lett.*, **112A** (1985).

[5] M.G. Forest, S. Pagano, R.D. Parmentier, P.L. Christiansen, M.P. Sorensen, and S.-P. Sheu, Numerical Evidence for Global Bifurcations Leading to Switching Phenomena in Long Josephson Junctions, *Wave Motion*, **12**, (1990), pp. 213-226.

[6] M.J. Friedman and E.J. Doedel, Numerical computation and continuation of invariant manifolds connecting fixed points, *SIAM J. Numer. Anal.*, **28**, (1991), pp. 789-808.

[7] A.D. Jepson and H.B. Keller, Steady State and Periodic Solution Paths: their Bifurcations and Computations, *Bifurcation: Analysis, Algorithms and Applications*, T. Kupper, H.D. Mittelmann and H. Weber, eds. (Birkhauser ISNM series, no. 70, 1984), pp. 219–246.

[8] H.B. Keller, Numerical Solution of Bifurcation and Nonlinear Eigenvalue Problems, *Applications of Bifurcation Theory*, P.H. Rabinowitz, ed. (Academic Press 1977), pp. 359–384.

[9] H.-O. Kreiss, *personal communication* (1990).

[10] M. Lentini and H.B. Keller, Boundary Value Problems over semi-infinite intervals and their numerical solution, *SIAM J. Numer. Anal.*, **17**, (1980), pp. 577-604.

[11] R.M. Miura, Accurate Computation of the Stable Solitary Wave for the FitzHugh-Nagumo Equations, *J. Math Biology*, **13**, (1982), pp. 247-269.

[12] S. Pagano, M.P. Soerensen, P.L. Christiansen, and R.D. Parmentier, Stability of fluxon motion in long Josephson junctions at high bias, *Phys. Rev. B*, **38**, (1988), pp. 4677-4687.

[13] N. A. Petersson, Computing Periodic Gravity Waves on Water by using Moving Composite Overlapping Grids, (CAM-report 92-01, Dept. of Mathematics, University of California, Los Angeles, CA, 1992).